

High- p_T Signatures in Vector–Leptoquark Models

Michael J. Baker, Javier Fuentes-Martín, Gino Isidori, Matthias König

Physik-Institut, Universität Zürich, CH-8057 Zürich, Switzerland

Abstract

We present a detailed analysis of the collider signatures of TeV-scale massive vector bosons motivated by the hints of lepton flavour non-universality observed in B -meson decays. We analyse three representations that necessarily appear together in a large class of ultraviolet-complete models: a colour-singlet (Z'), a colour-triplet (the U_1 leptoquark), and a colour octet (G'). Under general assumptions for the interactions of these exotic states with Standard Model fields, including in particular possible right-handed and flavour off-diagonal couplings for the U_1 , we derive a series of stringent bounds on masses and couplings that constrain a wide range of explicit new-physics models.

1 Introduction

The hints of Lepton Flavour Universality (LFU) violation in semi-leptonic B decays, namely the deviations from τ/μ (and τ/e) universality in $b \rightarrow c l \bar{\nu}$ decays [1–4] and the deviations from μ/e universality in $b \rightarrow s l \bar{l}$ decays [5, 6], are among the most interesting departures from the Standard Model (SM) reported by experiments in the last few years. The attempt to find a single beyond-the-SM (BSM) explanation for the combined set of anomalies has triggered intense theoretical activity, whose interest goes beyond the initial phenomenological motivation. In fact, it has shed light on new classes of SM extensions that turn out to be very interesting *per se* and that have not been investigated in great detail so far, pointing to non-trivial dynamics at the TeV scale possibly linked to a solution of the SM flavour puzzle.

The initial efforts to address both sets of anomalies have been focused on Effective Field Theory (EFT) approaches via four-fermion effective operators (see [7–10] for the early attempts). However, the importance of complementing EFT approaches with appropriate simplified models with new heavy mediators was soon realised [9, 11]. Given the relatively low scale of new physics hinted by the charged-current anomalies, the impact of considering a full model rather than an EFT on high- p_T constraints are significant [12–14]. More recently, a further advancement has been achieved with the development of more complete (and more complex) models with a consistent ultraviolet (UV) behaviour (see in particular [15–27]).

In early EFT attempts, it was realised that a particularly good mediator accounting for both sets of anomalies is a TeV-scale $U_1 \sim (\mathbf{3}, \mathbf{1}, 2/3)$ vector leptoquark, coupled mainly to third-generation fermions [8, 11]. The effectiveness of this state as a single mediator accounting for all available low-energy data has been clearly established in [28]. However, this state can not be the only TeV-scale vector particle in a realistic extension of the SM. Since it is a massive vector, the U_1 can be either a massive gauge boson of a spontaneously broken gauge symmetry $G_{\text{NP}} \supset G_{\text{SM}}$, as in the attempts

proposed in [15–18], or a vector resonance of some new strongly interacting dynamics, as e.g. in [19, 21]. As we show, in both cases the consistency of the theory requires additional vector states with similar masses. The purpose of this paper is to provide a comprehensive analysis of the high- p_T constraints on the vector leptoquark U_1 and what can be considered its minimal set of vector companions, namely a colour octet $G' \sim (\mathbf{8}, \mathbf{1}, 0)$, which we will refer to as the coloron, and a colour singlet $Z' \sim (\mathbf{1}, \mathbf{1}, 0)$.

In our analysis we consider the most general chiral structure for the U_1 couplings to SM fermions. This is in contrast with many recent studies which considered only left-handed (LH) couplings. While this hypothesis is motivated by the absence of clear indications of right-handed (RH) currents in the present data and by the sake of minimality, it does not have a strong theoretical justification. Indeed, the quantum numbers of the U_1 allow for RH couplings, and in motivated UV completions such couplings naturally appear [18, 26]. We also analyse the impact of a non-vanishing mixing between the second and third family in high- p_T searches, including in particular constraints from $pp \rightarrow \tau\mu$ and $pp \rightarrow \tau\nu$. As we show, the inclusion of right-handed couplings and/or a sizeable 2-3 family mixing yields significant modifications to the results found in the existing literature.

The structure of this paper is as follows: In section 2 we motivate our choice of TeV-scale vectors and in section 3 we introduce the phenomenological Lagrangian adopted to describe their high- p_T signatures. We then present the results of the searches in section 4 and conclude with section 5.

2 The spectrum of vector states at the TeV scale

The bottom-up requirement for the class of models we are interested in is the following effective interaction of the U_1 field with SM fermions:

$$\begin{aligned} \mathcal{L}_{\text{NP}} &\supset \frac{g_U}{\sqrt{2}} U_1^{\mu, \alpha} [(J_U^L)_{\mu}^{\alpha} + (J_U^R)_{\mu}^{\alpha}] + \text{h.c.} , \\ (J_U^L)_{\mu}^{\alpha} &= \beta_L^{ij} \bar{q}_L^{i, \alpha} \gamma_{\mu} \ell_L^j , \quad (J_U^R)_{\mu}^{\alpha} = \beta_R^{ij} \bar{d}_R^{i, \alpha} \gamma_{\mu} e_R^j . \end{aligned} \quad (1)$$

Here q_L (ℓ_L) denotes the left-handed quark (lepton) doublets, d_R (e_R) denotes the right-handed down-type quark (charge-lepton) singlets, $i \in \{1, 2, 3\}$ and $j \in \{1, 2, 3\}$ are flavour indices, $\alpha \in \{1, 2, 3\}$ is a $SU(3)_c$ index, and $\beta_{L,R}^{ij}$ are complex matrices in family-space.

The effective interaction in eq. (1) unambiguously identifies the representation of U_1 under $G_{\text{SM}} = SU(3)_c \times SU(2)_L \times U(1)_Y$ to be $(\mathbf{3}, \mathbf{1}, 2/3)$. There are two basic classes of well-defined UV theories where such interactions can occur:

- i. *Gauge models.* Here U_1 is the massive gauge boson of a spontaneously broken gauge symmetry $G_{\text{NP}} \supset G_{\text{SM}}$. The need for extra massive vectors follows from the size of the coset-space of $G_{\text{NP}}/G_{\text{SM}}$, that necessarily requires additional generators besides the six associated to U_1 .
- ii. *Strongly interacting models.* Here U_1 appears as a massive resonance for a new strongly interacting sector. In this case the need of additional massive vectors is a consequence of the additional resonances formed by the same set of constituents leading to U_1 .

Gauge models: the need for a Z'

Within gauge models, let us start analysing the case of a single generation of SM fermions ($i = j = 3$), and further assume that SM fermions belong to well-defined representations of G_{NP} (i.e. no mixing between SM-like and exotic fermions). Under these assumptions, β_L is non-zero only if q_L and ℓ_L belong to the same G_{NP} representation. We denote this representation ψ_L and, without loss of generality, we decompose it as

$$\psi_L = \psi_L^{\text{SM}} + \psi_L^{\text{exotic}} , \quad \psi_L^{\text{SM}} = \begin{pmatrix} q_L^{\beta} \\ \ell_L \end{pmatrix} . \quad (2)$$

In this notation the left-handed current in eq. (1) can be written as $(J_U^L)_\mu^\alpha = \bar{\psi}_L^{\text{SM}}(T_+^\alpha)\gamma_\mu\psi_L^{\text{SM}}$ with the following explicit expression for the action of the G_{NP} generators on the SM projection of ψ_L :

$$T_+^\alpha = \begin{pmatrix} 0 & \delta_{\alpha\beta} \\ 0 & 0 \end{pmatrix}. \quad (3)$$

The closure of the algebra of the six generators T_\pm^α associated with the six components of U_1 implies the need of the following additional (colour-neutral) generator

$$T_{B-L} = \begin{pmatrix} \frac{1}{3}\delta_{\beta\gamma} & 0 \\ 0 & -1 \end{pmatrix}, \quad \frac{1}{3} \sum_{\alpha,\delta=1}^3 [T_+^\alpha, T_-^\delta] = T_{B-L}. \quad (4)$$

The same conclusion is reached by looking at the right-handed coupling in eq. (1). Moreover, since a possible mixing between SM and exotic fermions must occur in a $SU(3)_c$ invariant way, the decomposition in eq. (2) also holds for possible exotic fermions mixing with the SM ones. Hence the need of T_{B-L} for the closure of the algebra is a general conclusion that holds independently of the possible mixing among fermion representations.

An equivalent way to deduce the need for an extra generator is the observation that the minimal group $G_{\text{NP}}^{\text{min}} \supset G_{\text{SM}}$ containing generators associated to the representation $(\mathbf{3}, \mathbf{1}, 2/3)$ is

$$G_{\text{NP}}^{\text{min}} = SU(4) \times SU(2)_L \times U(1)_{T_R^3}, \quad (5)$$

i.e. the subgroup of the Pati-Salam group $G_{\text{PS}} = SU(4) \times SU(2)_L \times SU(2)_R$ [29]. $G_{\text{NP}}^{\text{min}}$ is obtained by considering the $U(1)$ subgroup of $SU(2)_R$ defined by its diagonal (electric-charge neutral) generator T_R^3 . The coset $G_{\text{NP}}^{\text{min}}/G_{\text{SM}}$ contains seven generators: the six T_\pm^α describing the coset $SU(4)/SU(3)_c \times U(1)_{B-L}$, and T_{B-L} .

In gauge models, the presence of an extra massive vector $Z' \sim (\mathbf{1}, \mathbf{1}, 0)$ associated with the breaking $U(1)_{B-L} \times U(1)_{T_R^3} \rightarrow U(1)_Y$ is thus unavoidable. Since the breaking of $U(1)_{B-L}$ necessarily implies a breaking of $SU(4)$, the breaking terms which lead to a non-vanishing Z' mass necessarily induce a mass term for the U_1 as well. Hence, the Z' state cannot be decoupled. The opposite is not true: since the U_1 generators are associated to the $SU(4)/SU(3)_c \times U(1)_{B-L}$ coset, mass terms for the U_1 do not necessarily contribute to the Z' mass.

Gauge models: the need for a G'

While the minimal group in eq. (5) allows us to build a consistent model for a massive $U_1 \sim (\mathbf{3}, \mathbf{1}, 2/3)$, it does not leave us enough freedom to adjust U_1 and Z' couplings in order to comply with low- and high-energy data.

Under $G_{\text{NP}}^{\text{min}}$ the interaction strengths of both U_1 and Z' are unambiguously related to the QCD coupling (g_s) and to hypercharge, given that they all originate from the same $SU(4)$ group. In particular $g_U = g_s(M_{U_1})$, in a normalisation where $|\beta_{L,R}^{ij}| \leq 1$. Moreover, the couplings of the Z' to SM fermions are necessarily flavour universal.¹ A flavour-universal Z' is constrained by LHC dilepton searches to have $M_{Z'} \gtrsim 5$ TeV [30, 31]. Within $G_{\text{NP}}^{\text{min}}$, the U_1 should be necessarily close in mass [22] which, together with the low value of g_U , results in a negligible impact on $b \rightarrow c\ell\nu$ decays.

To avoid these constraints, T_\pm^α , T_{B-L} , and the QCD generators T^a , should not be unified in a single $SU(4)$ group. Given the commutation rules between T_\pm^α and T^a , the next-to-minimal option is obtained with [15]

$$(G_{\text{NP}}^{\text{min}})' = SU(4) \times SU(3)' \times SU(2)_L \times U(1)_{T_R^3}, \quad (6)$$

¹This statement follows from the fact that the mixing of SM fermions among themselves (in flavour space) and with possible exotic representations necessarily involve states with the same $B - L$ charges. As a result, the mixing acts as a unitary rotation on the Z' couplings that remains proportional to the identity matrix in flavour space.

where $SU(3)_c$ is the diagonal subgroup of $SU(4) \times SU(3)'$ (see also [32, 33]). In this case we can achieve the two goals of 1) decoupling the overall coupling of U_1 from g_c , letting it reach the higher values needed to impact B -physics data with $M_{U_1} \sim$ few TeV; 2) having flavour non-universal couplings for both U_1 and Z' . The latter can be achieved either via mixing with exotic fermions (as in [15]), and/or with a flavour-dependent assignment of the $SU(4) \times SU(3)'$ quantum numbers (as in [18, 20]).

The enlargement of the coset space to $(G_{\text{NP}}^{\text{min}})' / G_{\text{SM}}$ directly requires a massive colour-octet vector (the “coloron” G') associated to the breaking $SU(3)_{[4]} \times SU(3)'$, where $SU(3)_{[4]}$ is the “coloured” subgroup of $SU(4)$. Similarly to the case of the Z' , breaking terms leading to a non-vanishing G' mass necessarily induces a mass term also for the U_1 , while the opposite is not necessarily true.

Vector spectrum in strongly interacting models

In strongly interacting models, the leptoquark U_1 is a composite state with two elementary fermions charged under the new confining group G_{strong} as constituents. These fermions are necessarily charged under $SU(3)_c$ in order to generate a colour-triplet state.

The simplest option is the case of a vector triplet (χ_q^α) and a vector singlet (χ_ℓ), both in the fundamental of G_{strong} , such that

$$\langle 0 | \bar{\chi}_q^\alpha \gamma_\mu \chi_\ell | U_1(p, \epsilon) \rangle = F_U \epsilon_\mu^\alpha , \quad (7)$$

where we have not explicitly indicated the G_{strong} indices. With these basic constituents one expects also one G' and two Z' :

$$\langle 0 | \bar{\chi}_q^\alpha T_{\alpha\beta}^a \gamma_\mu \chi_q^\beta | G(p, \epsilon) \rangle = F_{G'} \epsilon_\mu^a , \quad \langle 0 | \bar{\chi}_q^\alpha \gamma_\mu \chi_q^\alpha | Z'_q(p, \epsilon) \rangle = F_{Z'_q} \epsilon_\mu , \quad \langle 0 | \bar{\chi}_\ell \gamma_\mu \chi_\ell | Z'_\ell(p, \epsilon) \rangle = F_{Z'_\ell} \epsilon_\mu . \quad (8)$$

The masses of these states are not precisely related to that of the U_1 as in the case of gauge models, but they are expected to be of similar size since they originate from the same dynamics. In principle one can enlarge the multiplicity of the constituents, e.g. the colour triplet U_1 can be achieved by combining **3** and **8** of $SU(3)_c$, but this can only increase the number of extra coloured vectors. A further exotic option is to consider U_1 as a fermion bilinear in an antisymmetric combination of G_{strong} , as allowed e.g. in $SU(2)$. However, beside this peculiar case where symmetric G_{strong} combinations are forbidden (or much heavier in mass), this does not prevent the presence of at least one G' and one Z' with masses comparable to the U_1 .

3 Phenomenological Lagrangian

Having motivated the minimal set $\{G', Z', U_1\}$ of massive vectors for a meaningful description of TeV scale dynamics, we proceed to set up a versatile framework for analysing the high- p_T signatures of these states in a general way. In our analysis we restrict our attention to the interactions of these vectors with SM fermions and gauge bosons. We neglect possible Higgs couplings to the Z' since they are severely constrained by electroweak precision data (see e.g. [28]) and are typically very small in the model realisations we are interested in. We also ignore any possible interactions of the extra vectors among themselves and to any other particles related to the UV completion of the model (either scalars or fermions). While some of the high- p_T signatures related to these interactions can be quite interesting [22], they are highly dependent on the details of the UV completion. Here we only consider their possible indirect effects on the widths of the vectors, which we treat as an additional free parameter.²

²We will consistently assume that right-handed neutrinos, if present, are heavy enough so that they effectively decouple and do not play any relevant role. Models with light ν_R in connection to the B -anomalies can be found in [34–37], and in connection to the vector leptoquark in [38].

We define the general Lagrangian for these vectors as follows:

$$\begin{aligned}\mathcal{L}_{U_1} = & -\frac{1}{2} U_{1\mu\nu}^\dagger U_1^{\mu\nu} + M_U^2 U_{1\mu}^\dagger U_1^\mu - ig_s (1 - \kappa_U) U_{1\mu}^\dagger T^a U_{1\nu} G^{a\mu\nu} \\ & - ig_Y \frac{2}{3} (1 - \tilde{\kappa}_U) U_{1\mu}^\dagger U_{1\nu} B^{\mu\nu} + \frac{g_U}{\sqrt{2}} [U_1^\mu (\beta_L^{ij} \bar{q}_L^i \gamma_\mu \ell_L^j + \beta_R^{ij} \bar{d}_R^i \gamma_\mu e_R^j) + \text{h.c.}],\end{aligned}\quad (9)$$

$$\begin{aligned}\mathcal{L}_{Z'} = & -\frac{1}{4} Z'_{\mu\nu} Z'^{\mu\nu} + \frac{1}{2} M_{Z'}^2 Z'_\mu Z'^\mu + \frac{g_{Z'}}{2\sqrt{6}} Z'^\mu (\zeta_q^{ij} \bar{q}_L^i \gamma_\mu q_L^j + \zeta_u^{ij} \bar{u}_R^i \gamma_\mu u_R^j \\ & + \zeta_d^{ij} \bar{d}_R^i \gamma_\mu d_R^j - 3 \zeta_\ell^{ij} \bar{\ell}_L^i \gamma_\mu \ell_L^j - 3 \zeta_e^{ij} \bar{e}_R^i \gamma_\mu e_R^j),\end{aligned}\quad (10)$$

$$\begin{aligned}\mathcal{L}_{G'} = & -\frac{1}{4} G'_{\mu\nu}^a G'^{a\mu\nu} + \frac{1}{2} M_{G'}^2 G'_\mu^a G'^{a\mu} + \frac{1}{2} \kappa_{G'} G'_{\mu\nu}^a G^{a\mu\nu} + g_s \tilde{\kappa}_{G'} f_{abc} G'_\mu^a G'^b_\nu G^{c\mu\nu} \\ & + g_{G'} G'^{a\mu} (\kappa_q^{ij} \bar{q}_L^i T^a \gamma_\mu q_L^j + \kappa_u^{ij} \bar{u}_R^i T^a \gamma_\mu u_R^j + \kappa_d^{ij} \bar{d}_R^i T^a \gamma_\mu d_R^j),\end{aligned}\quad (11)$$

where $T^a = \lambda^a/2$, with λ^a ($a = 1, \dots, 8$) the Gell-Mann matrices. In both \mathcal{L}_{U_1} and $\mathcal{L}_{G'}$ we include possible non-minimal interactions with SM gauge fields, which play a role in the pair production of the heavy vectors at the LHC. In gauge models these couplings vanish, $\kappa_U = \tilde{\kappa}_U = \kappa_{G'} = \tilde{\kappa}_{G'} = 0$. However, this is not necessarily the case in strongly interacting models. The so-called minimal-coupling scenario for the leptoquark corresponds to $\kappa_U = \tilde{\kappa}_U = 1$. Since a triple coupling of the type GGG' would lead to a huge enhancement of the colour-octet production at LHC and with that, to very strong constraints from high-energy data, in what follows we will take $\kappa_{G'} = 0$.

Without loss of generality, we choose the flavour basis of the $SU(2)_L$ fermion doublets to be aligned to the down-quark sector, i.e.

$$q_L^i = \begin{pmatrix} V_{ji}^* u_L^j \\ d_L^i \end{pmatrix}, \quad \ell_L^i = \begin{pmatrix} \nu_L^i \\ e_L^i \end{pmatrix}, \quad (12)$$

where V_{ji} denote the CKM matrix elements. We assume that the new vectors are coupled dominantly to third generation fermions. The couplings to light quarks are assumed to respect a $U(2)_q$ flavour symmetry broken only in the leptoquark sector by the same leading spurion controlling the $3 \rightarrow q$ mixing in the CKM matrix [39]. We parameterise the strength of this spurion by β_L^{23} . In the lepton sector we assume vanishing couplings to electrons. These assumptions are phenomenologically motivated by the tight constraints from low-energy observables, in particular $\Delta F = 2$ amplitudes and lepton flavour violation in charged leptons (see e.g. [26, 28]). More precisely, we take the following textures for the vector couplings ($Q = q, u, d$):

$$\begin{aligned}\beta_L = & \begin{pmatrix} 0 & 0 & \beta_L^{13} \\ 0 & 0 & \beta_L^{23} \\ 0 & \beta_L^{32} & \beta_L^{33} \end{pmatrix}, \quad \beta_R = \text{diag}(0, 0, \beta_R^{33}), \\ \zeta_\ell = & \begin{pmatrix} 0 & 0 & 0 \\ 0 & \zeta_\ell^{22} & \zeta_\ell^{23} \\ 0 & (\zeta_\ell^{23})^* & \zeta_\ell^{33} \end{pmatrix}, \quad \zeta_e = \text{diag}(0, \zeta_e^{22}, \zeta_e^{33}), \\ \zeta_Q = & \text{diag}(\zeta_Q^{ll}, \zeta_Q^{ll}, \zeta_Q^{33}), \quad \kappa_Q = \text{diag}(\kappa_Q^{ll}, \kappa_Q^{ll}, \kappa_Q^{33}).\end{aligned}\quad (13)$$

As shown in [28], the assumption of a single $U(2)_q$ breaking spurion in both leptoquark and SM Yukawa couplings implies the relation $\beta_L^{13} = V_{td}^* / V_{ts}^* \beta_L^{23}$.

Constrained BSM amplitude	Final state	Data set	Section	Reference
U_1 pair prod.	$b\bar{b}\tau^-\tau^+$	CMS, 35.9 fb^{-1}	4.1	[40]
U_1 pair prod.	$t\bar{t}\nu_\tau\bar{\nu}_\tau$	CMS, 35.9 fb^{-1}	4.1	[41]
G' pair prod.	$2b2\bar{b}$	CMS, 35.9 fb^{-1}	4.1	[42]
U_1 [t chan.] & Z' [s chan.]	$\tau_h^+\tau_h^-$	ATLAS, 36.1 fb^{-1}	4.2	[43]
U_1 [t chan.]	$\tau_h\nu$	CMS, 35.9 fb^{-1}	4.3	[44]
U_1 [t chan.] & Z' [s chan.]	$\tau_h\mu$	ATLAS, 36.1 fb^{-1}	4.4	[45]
G' [s chan.] & Z' [s chan.]	$t\bar{t}$	ATLAS, 36.1 fb^{-1}	4.5	[46]

Table 1: Summary of the relevant experimental constraints. All searches have a centre of mass energy of 13 TeV.

4 Results

We consider a variety of high- p_T searches at the LHC which place limits on the model discussed above. The most constraining ones, which we discuss in detail below, are shown in table 1. In some cases the searches are optimised for the BSM processes we are interested in, allowing a simple translation of the reported limits in terms model parameters. In most cases however, a reinterpretation of the reported limits is necessary.

A relatively simple case is that of the leptoquark pair production. The differential and total cross-sections for these processes are well-known [47]. Here we use the recent CMS analyses dedicated to pair-produced (scalar) leptoquarks decaying primarily to third generation SM fermions [40, 41]. Since the leptoquarks are predominantly produced via their strong couplings to gluons, the limits only depend on the branching ratios to the relevant final states. Bounds on the coloron mass are extracted from a search for pair-produced resonances decaying to quark pairs, reported by CMS in the same way [42].

The case of the $\tau^+\tau^-$ final state, which constrains both the Z' (s channel production) as well as the U_1 (t channel exchange), is significantly more involved. Here we re-interpret the limits on resonances decaying into tau-lepton pairs, with hadronically decaying taus, reported by ATLAS [43]³ (bounds from leptonic tau decays turn out to be significantly weaker at large ditau invariant masses). We first consider the bounds placed on the U_1 and on the Z' in isolation, for various choices of couplings and widths, and then in combination. As we emphasise below, it is essential to include all relevant experimental information when deriving limits in this case.

We extract further bounds on U_1 by recasting CMS searches for $pp \rightarrow \tau\nu$ [44] and limits on both Z' and U_1 from the $pp \rightarrow \tau\mu$ search by ATLAS [45]. In both cases the 2-3 family mixing of the leptoquark plays a key role. As far as other dilepton final states are concerned, we explicitly checked that constraints from $pp \rightarrow \mu\mu$ (see e.g. [31]) do not significantly constrain the parameter space relevant to our model.

The leading bound on the G' is extracted by the unfolded $t\bar{t}$ invariant mass spectrum provided by ATLAS [46]. In principle, the U_1 and the Z' could be constrained by dijet searches. However, in our setup resonances tend to be very wide, with a width-over-mass $\sim 25\%$. As a result, the limits reported in the literature on narrow dijet peaks over a data driven background spectrum [49–51] are not directly applicable. Furthermore, dijet signatures are mostly produced for light quarks and

³We do not consider the corresponding analysis by CMS [48], which focuses on heavy Higgs bosons.

Parameters		$b\bar{b}\tau^-\tau^+$ final state		$t\bar{t}\nu_\tau\bar{\nu}_\tau$ final state	
κ_U	β_R^{33}	$\text{BR}(U_1 \rightarrow b\tau^+)$	Limit [TeV]	$\text{BR}(U_1 \rightarrow t\bar{\nu}_\tau)$	Limit [TeV]
0	0	0.51	1.4	0.50	1.6
0	1	0.67	1.5	0.33	1.3
1	0	0.51	1.1	0.49	1.1
1	1	0.67	1.2	0.32	1.0

Table 2: Summary of the experimental constraints on pair produced leptoquarks in the $b\bar{b}\tau^-\tau^+$ [40] and $t\bar{t}\nu_\tau\bar{\nu}_\tau$ [41] final states, assuming the leptoquarks decay solely into third generation SM particles.

gluons, which couple only weakly to Z' and G' in our setup.⁴ Indeed, dedicated recasts of dijet searches performed in a setup similar to ours have shown that these constraints are less significant than those from the $t\bar{t}$ final state [22]. Although one can envision scenarios where current dijet searches are more constraining than $t\bar{t}$ searches, such as when third-generation couplings are suppressed or when light-generation couplings are large, these limits are less relevant for the class of models which fit the flavour anomalies and so we do not consider dijet searches.

To perform recasts of these searches we implement the model described in section 3 in `FeynRules 2.3.32` [54] and generate the corresponding UFO model file. The `FeynRules` model files as well as the corresponding UFO model are available at <https://feynrules.irmp.ucl.ac.be/wiki/LeptoQuark>. In our `FeynRules` implementation and in all our results throughout this paper, we include only tree-level effects. While some NLO QCD corrections are available for the vector leptoquark case [55], in specific models these are expected to be supplemented by additional NLO contributions that can be of similar (or even larger) size. Hence we opt not to include them and we add a systematic error in our signal to (partially) account for them. Other `FeynRules` implementations for the vector leptoquark (but with interactions to third-generation left-handed fields only) are available [56]. We have cross-checked our leptoquark implementation (with $\beta_R^{33} = 0$) against the one in [56], finding a perfect agreement between the two.

4.1 Limits from resonance pair production

We first briefly discuss limits on the leptoquark coming from their pair production. The dominant production modes are governed by QCD and the relevant couplings are the strong gauge coupling and κ_U , see eq. (13). The limits then depend on κ_U , the leptoquark mass and its branching ratio into the given final states. The most constraining searches in our scenario are those for the $b\bar{b}\tau^-\tau^+$ [40] and $t\bar{t}\nu_\tau\bar{\nu}_\tau$ [41] final states.

In table 2 we report the limits for various values of κ_U and β_R^{33} , which determines the branching ratios (the branching ratios deviate slightly from the expected 1/2, 1/3, 2/3 due to phase space effects). We assume that the leptoquark decays only into third generation SM particles and find that the limits range from 1 TeV to 1.6 TeV. Similar limits have also been obtained in the literature, see e.g. [33, 41, 57], although using lower luminosity in the $b\bar{b}\tau^-\tau^+$ channel. Whenever it is possible to compare, we find good agreement between our results and those in the aforementioned references. With $\kappa_U = 0$ there is an extra coupling to the gluon field strength tensor boosting the production cross-section and strengthening the limit. As β_R^{33} increases, the branching ratio to $b\tau^+$ increases while the branching ratio to $t\bar{\nu}_\tau$ decreases, which is reflected in a strengthening and weakening of

⁴Searches for b -tagged dijet signatures would remedy this, but they tend to be sensitive to relatively low mass ranges and narrow widths [52, 53].

Particle selection	At least two τ_h 's and no electrons or muons
Charge	$\tau_{h1} \tau_{h2}$ should be of opposite charge
$\tau_h p_T$	$p_T^{\tau_{h1}} > 130 \text{ GeV}, p_T^{\tau_{h2}} > 65 \text{ GeV}$
η	$ \eta_{\tau_h} < 2.5$ excluding $1.37 < \eta_{\tau_h} < 1.52$
ϕ	$ \Delta\phi(\tau_{h1}, \tau_{h2}) > 2.7 \text{ rad}$

Table 3: Summary of the experimental cuts for the ATLAS $\tau_h \tau_h$ search [43]. For the leading τ_h we use the p_T cut $p_T^{\tau_{h1}} > 130 \text{ GeV}$ as quoted in the HEPData entry for Ref. [43]. Note that the corresponding cut was $p_T^{\tau_{h1}} > 85 \text{ GeV}$ for 10% of the data.

the limits, respectively. For illustration, we include the strongest bound from pair-production, i.e the limit $M_U > 1.6 \text{ TeV}$, in figs. 1, 6 and 7.

In a similar fashion, bounds on the coloron mass can be extracted from a search for pair-produced resonances decaying to quark pairs, performed by the CMS collaboration [42]. The search excludes a coloron in the whole mass range considered, from 80 GeV to 1500 GeV, so provides an upper bound of $M_{G'} > 1.5 \text{ TeV}$. However, a stronger upper bound can be estimated by extrapolating the production cross-section and exclusion limit to higher energies, where bounds of 1.7 TeV and 2.1 TeV for $\tilde{\kappa}_{G'} = 0$ and $\tilde{\kappa}_{G'} = 1$ are obtained. The stronger bound in the latter case can be understood from the fact that the corresponding operator in eq. (11) adds significantly to the $gg \rightarrow G'G'$ amplitude. The estimated limits are practically independent of the choices of the couplings to quarks, because the production cross section is dominated by the gluon-initiated processes. In setting these limits, we fix the coloron gauge coupling to $g_{G'} = 3$, $\kappa_{G'} = 0$ and $\kappa_{q,u,d}^{33} = 1$.

4.2 $pp \rightarrow \tau\tau$ search

The ATLAS collaboration has performed a search of heavy resonances in the ditau final state using 36.1 fb^{-1} of 13 TeV data [43]. In this section we recast this search to set limits on the U_1 and Z' masses for different choices of the couplings. In section 4.2.3 and section 4.2.2 we consider separate limits for the Z' and U_1 assuming that one of the two has fully decoupled. The interplay of the two resonances in this search is considered at the end, in section 4.2.4.

4.2.1 Search strategy

We focus on the analysis with $\tau_h \tau_h$ since this channel presents the highest sensitivity to high-mass resonances. The contributions to the $pp \rightarrow \tau^+ \tau^-$ process from new heavy resonances, including the interference with the SM, are computed using `Madgraph5_aMC@NLO v2.6.3.2` [58], with the `NNPDF23_lo_as_0119_qed` PDF set [59]. Hadronization of the τ final states is performed with `Pythia 8.2` [60] with the A14 set of tuned parameters. Detector simulation is done using `Delphes 3.4.1` [61]. The ATLAS Delphes card has been modified to satisfy the object reconstruction and identification requirements. In particular we include the τ -tagging efficiencies quoted in the experimental search [43]. After showering and detector simulation, we apply selection cuts using `MadAnalysis 5 v1.6.33` [62] (see table 3 for details on the applied cuts). We have validated our results by generating the SM Drell-Yan $pp \rightarrow \tau\tau$ background and comparing our results with the one quoted by ATLAS. A good agreement is found between the two samples (we find a discrepancy with the quoted central values of less than 20%, well within the given 1σ region).

After passing through selection cuts, the resulting events are binned according to their total transverse mass,

$$m_T^{\text{tot}} \equiv \sqrt{(p_T^{\tau_{h1}} + p_T^{\tau_{h2}} + E_T^{\text{miss}})^2 - (\vec{p}_T^{\tau_{h1}} + \vec{p}_T^{\tau_{h2}} + \vec{p}_T^{\text{miss}})^2}, \quad (14)$$

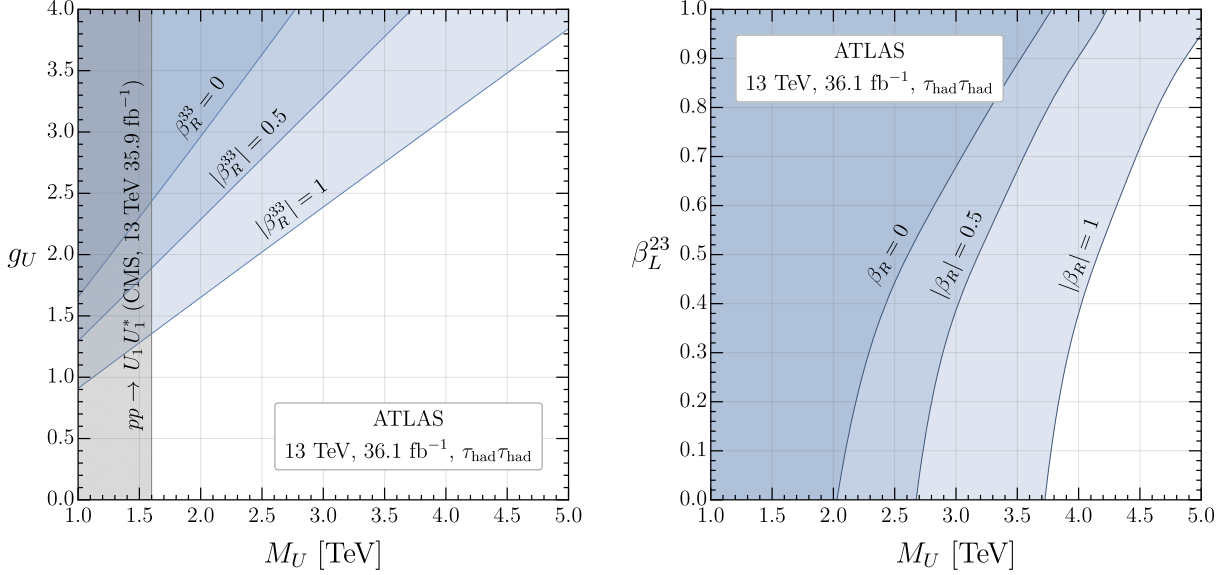


Figure 1: Exclusion plot for the $pp \rightarrow \tau\tau$ search in the (g_U, M_U) (left) and (β_L^{23}, M_U) (right) planes for different values of the coupling β_R^{33} . We fix $\beta_L^{33} = 1$ and the leptoquark width to its natural value. In the left plot we set $\beta_L^{23} = 0$ and, for comparison, we also show the limits from U_1 pair production. In the right plot we set $g_U = 3$.

where $p_T^{7h1,2}$ are the transverse momenta of the visible decay products for the leading and sub-leading taus, respectively, and E_T^{miss} and \vec{p}_T^{miss} are the total missing transverse energy and missing momentum in the reconstructed event. We compare our binned events with the histogram in Fig. 3b of the supplementary material of [43], which contains the corresponding m_T^{tot} histograms for the SM background and the experimental data, with b -tag inclusive event selection. For the statistical analysis we use the modified frequentist CL_s method [63]. We compute the CL_s using the `ROOT` [64] package `Tlimit` [65] and exclude model parameter values with $CL_s < 0.05$. In our statistical analysis we include all the bins and SM backgrounds errors, provided by the ATLAS collaboration in the corresponding HEPData entry [43].⁵ We also include a systematic uncertainty of 20% for the signal to account for possible uncertainties related to the PDF, tau hadronization, detector simulation and unaccounted NLO corrections.

4.2.2 Limits on the U_1 leptoquark

In this section we decouple the Z' and concentrate on the limits arising exclusively from the leptoquark exchange. In our search we take maximal values for β_L^{33} (i.e. $\beta_L^{33} = 1$) and consider three benchmarks for the right-handed coupling: $|\beta_R^{33}| = \{0.0, 0.5, 1.0\}$. Note that the search is not sensitive to the relative sign choice between β_R^{33} and β_L^{33} but only to their magnitudes. The reason for this is that the New Physics (NP) amplitudes of different chiralities do not interfere with each other and the amplitude proportional to $\beta_R^{33} \beta_L^{33}$ does not interfere with the SM ones. We further fix the leptoquark width to its natural value. The leptoquark width only mildly affects the results of this search, contrary to the Z' case discussed in the next section, since the NP contribution is generated via a t channel exchange.

Exclusion limits in the (g_U, M_U) plane, setting $\beta_L^{23} = 0$, are shown in fig. 1 (left). Similar recasts for the case with $\beta_L^{23} = 0$ can be found in the literature [57, 66]. We obtain slightly stronger limits

⁵The power of each of the bins in excluding a signal is shown in fig. 5, where we plot the 95% CL exclusion limit in the leptoquark mass, as a function of the number of the bins included in the statistical analysis.

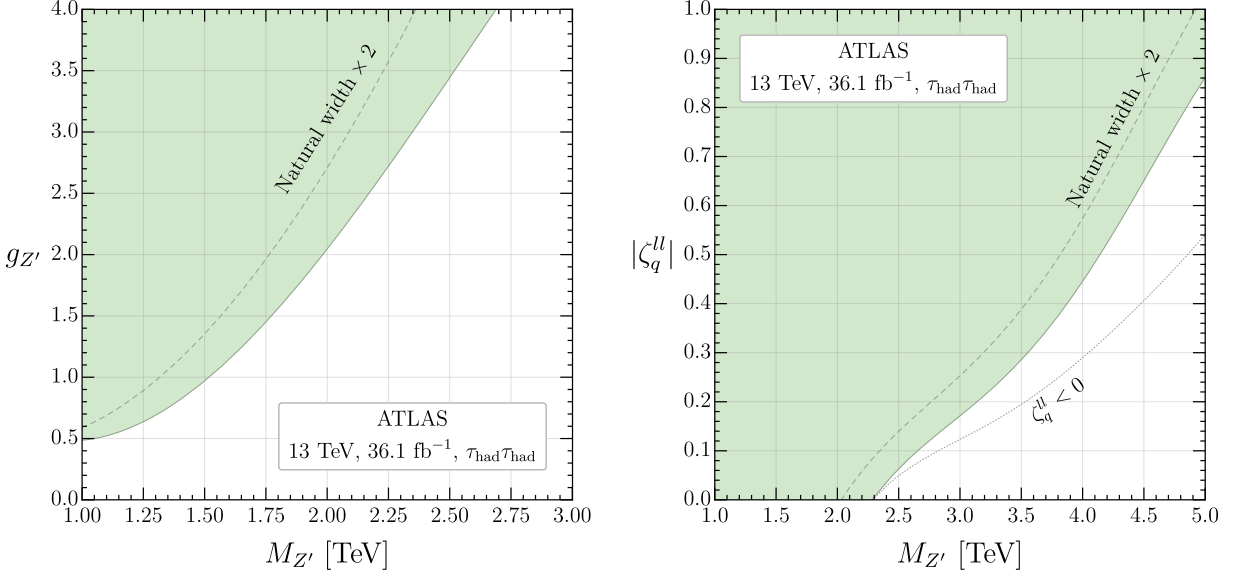


Figure 2: Exclusion plot for the $pp \rightarrow \tau\tau$ search in the $(g_{Z'}, M_{Z'})$ plane (left) and $(\zeta_q^{ll}, M_{Z'})$ plane (right), and for the natural width $\times 2$ while maintaining the natural partial width to tau pairs (dashed curves). In the left plot we set $\zeta_q^{ll} = 0$. In the right plot we set $g_{Z'} = 3$.

than those in the previous references. As we show in fig. 5, this difference can be understood from the fact that we consider the full m_T^{tot} distribution and not only the highest bin. The lower bins are important since a t channel exchange gives rise to a broad tail in the spectrum. Exclusion limits for the scenario where $\beta_R^{33} \neq 0$ have not been discussed in the literature. We find that the additional chirality significantly enhances the cross section, yielding limits that are about 70% stronger than in the case when $\beta_R^{33} = 0$.

Finally, we also study the limits on M_U for non-zero values of β_L^{23} , fig. 1 (right). Here we fix $g_U = 3$ and $\beta_L^{33} = 1$ and plot the corresponding exclusion limits for the three benchmark values of β_R^{33} discussed above. As can be seen, only a mild increase of the limits is found for $\beta_L^{23} \lesssim 0.4$. For larger values of β_L^{23} , the PDF enhancement is enough to make $s\bar{s} \rightarrow \tau^+\tau^-$ the dominant partonic channel and the limits start growing linearly with β_L^{23} .

4.2.3 Limits on the Z' resonance

We now proceed to the limits set on the Z' , decoupling the leptoquark. Throughout this section we fix $\zeta_{q,u,d}^{33} = \zeta_{\ell,e}^{33} = 1$ and focus on the impact of varying the overall Z' coupling $g_{Z'}$, varying the coupling to left-handed light quarks ζ_q^{ll} , and varying the width of the Z' .

In the left panel of fig. 2 we set $\zeta_q^{ll} = 0$ and show the exclusion in the $(g_{Z'}, M_{Z'})$ plane. For small couplings, $g_{Z'} < 0.5$, the Z' is not excluded above 1 TeV as the production cross section is too small. In the range $0.5 < g_{Z'} < 1.0$ the limit increases from 1 TeV to 2 TeV and it approaches a regime where it increases linearly with the coupling. This can be understood by the fact that, having set $\zeta_q^{ll} = 0$, the Z' is dominantly produced from b -quarks, which carry only low momentum fractions of the protons. As a result, even for relatively low masses the effective cross-section scales like a contact interaction $\sigma'_Z \sim g_{Z'}^{1/4}/M_{Z'}^{1/4}$.

Finally, we also show the impact of varying the width. As can be noted, doubling the width (dashed line in fig. 2) has a relatively minor impact. This is consistent with the observation that the limits does not come from the on-shell production of the Z' , but rather from its tail (that scales like a contact interaction).

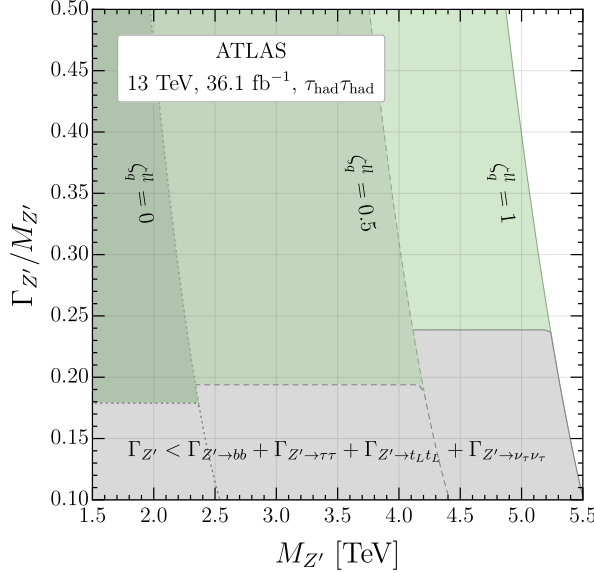


Figure 3: Exclusion plot for the $pp \rightarrow \tau\tau$ search in the $(\Gamma_{Z'}/M_{Z'}, M_{Z'})$ plane for $\zeta_q^{ll} = \{0.0, 0.5, 1.0\}$ for dotted, dashed and full lines, respectively. The grey area shows values of the width which are below the corresponding natural width.

In fig. 2 (right) we fix $g_{Z'} = 3$ and vary the couplings to left-handed light quarks ζ_q^{ll} . Since the light quarks have less PDF suppression than the third-generation quarks, the limit increases rapidly. For $\zeta_q^{ll} \ll 1$, the width is not affected by increasing ζ_q^{ll} , while for larger values of ζ_q^{ll} the width starts to be affected leading to a change of slope.

We again show that doubling the natural width decreases the limit by around 10 %. We also show the impact of changing the relative sign between the light quark couplings and the third-generation coupling. With opposite signs the interference term contributes constructively, strengthening the limit, whereas when the signs are the same the interference term contributes destructively, weakening the limit.

In fig. 3 we fix $g_{Z'} = 3$ and vary the width for $\zeta_q^{ll} \in \{0.0, 0.5, 1.0\}$. As noted above, we see that the limit depends only weakly on the width. For all values of ζ_q^{ll} , a doubling of the width from 25% to 50% decreases the limit by around 10%. The grey area show values of the width which are below the corresponding natural width.

In summary, the Z' mass limit of the ditau search depends weakly on the universal coupling $g_{Z'}$, is very sensitive to the light-quark couplings (it is excluded below 5 TeV for $\zeta_q^{ll} \approx 1$), and is only weakly relaxed by an increase of the total width of the Z' .

4.2.4 Combined limits for the Z' and the U_1 leptoquark

We now consider the limits when both the Z' and the leptoquark are present. For the Z' we set $\zeta_{q,u,d}^{33} = \zeta_{\ell,e}^{33} = 1$ and $\zeta_q^{ll} = 0$. For the leptoquark we set $\beta_L^{33} = \beta_R^{33} = 1$ and $\beta_L^{23} = 0$. In both cases we assume natural widths.

In fig. 4 we show the exclusion limit on the $(M_U, M_{Z'})$ plane for a variety of overall coupling strengths, $g_U = g_{Z'} \in \{2.5, 3.0, 3.5\}$. The increase of the limits with growing coupling in each step is relatively small for the Z' (~ 200 GeV), while it is larger for the leptoquark (~ 600 GeV). We see that the decoupling regimes considered in the previous two sections hold when the Z' is heavier than (roughly) 3 TeV, and when the leptoquark is heavier than 5 – 6 TeV.

Below the decoupling regime, the limits on both particles strengthen by a few hundred GeV, since they both contribute to the m_T^{tot} distribution.

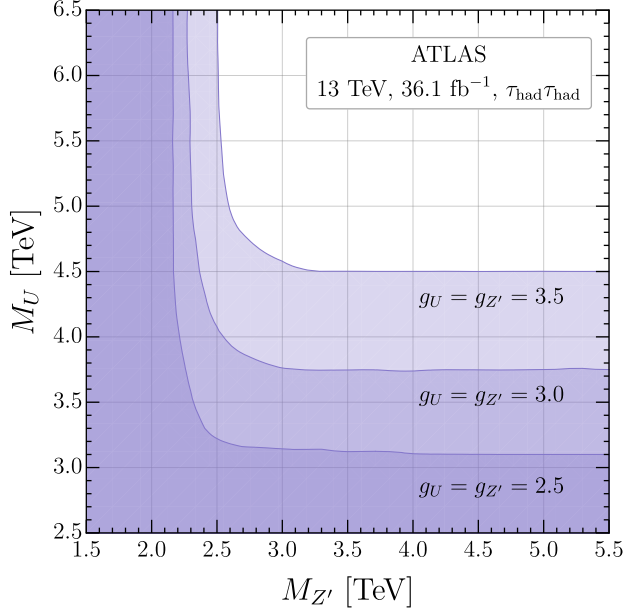


Figure 4: 95% CL exclusion limits from the $pp \rightarrow \tau\tau$ search in the $(M_U, M_{Z'})$ plane for different values of the gauge couplings $g_U = g_{Z'}$. All couplings to light quarks are set to zero.

We now highlight the importance of including more than just the highest bin in m_T^{tot} in setting the mass limit. In fig. 5 (left) we plot the m_T^{tot} distribution of the data and background from [43], along with our simulated leptoquark and Z' contributions. We show the distributions for $g_U = 3$ and $g_{Z'} = 3$, for masses at the 95% C.L. limit. After a peak, the background steadily falls with increasing m_T^{tot} . The final bin has a larger number of events than the preceding bin as this bin is wider and as it includes overflow events. As such, the final three bins each contain a similar number of background events. Since tau pair production via a Z' proceeds through an s channel, it is more peaked in m_T^{tot} and the events from a multi-TeV Z' cluster in the highest energy bin. However, tau pair production via a leptoquark proceeds through t channel process, so there is no clear peak in the invariant mass distribution. This leads the distribution in m_T^{tot} to extend to lower values. We see in fig. 5 (right) the impact of including only the N highest bins in the CLs calculation. For the Z' , the limit obtained with only the highest bin is almost 200 GeV lower than the limit including all bins. For the leptoquark, when only the highest bin is included, the 95% C.L. limit is around 400 GeV weaker than when all bins are included. When the highest two bins are included the difference reduces to around 100 GeV, and slowly improves as more bins are added. We see that it is crucial to include more than the highest bin in m_T^{tot} to produce an accurate estimate of the leptoquark exclusion limit.

4.3 $pp \rightarrow \tau\nu$ search

The ATLAS and CMS collaborations have performed searches for heavy resonances decaying to $\tau\nu$ (with hadronically decaying τ) using 36.1 fb^{-1} [67] and 35.9 fb^{-1} [44] of 13 TeV data, respectively. In this section we reinterpret this search in the context of the model in section 3 to set limits on the vector leptoquark mass as a function of β_{23}^L . In our limits we use the CMS data. Since ATLAS data presents a (small) upper fluctuation with respect to the SM background, a combination of ATLAS and CMS data yields slightly weaker limits than CMS data alone (see e.g. [14]).

4.3.1 Search strategy

We compute the NP contribution to the $pp \rightarrow \tau_h \nu$ process, including the interference with the SM, using `Madgraph5_aMC@NLO v2.6.3.2` [58], with the `NNPDF23_lo_as_0119_qed` PDF set [59]. Hadroniza-

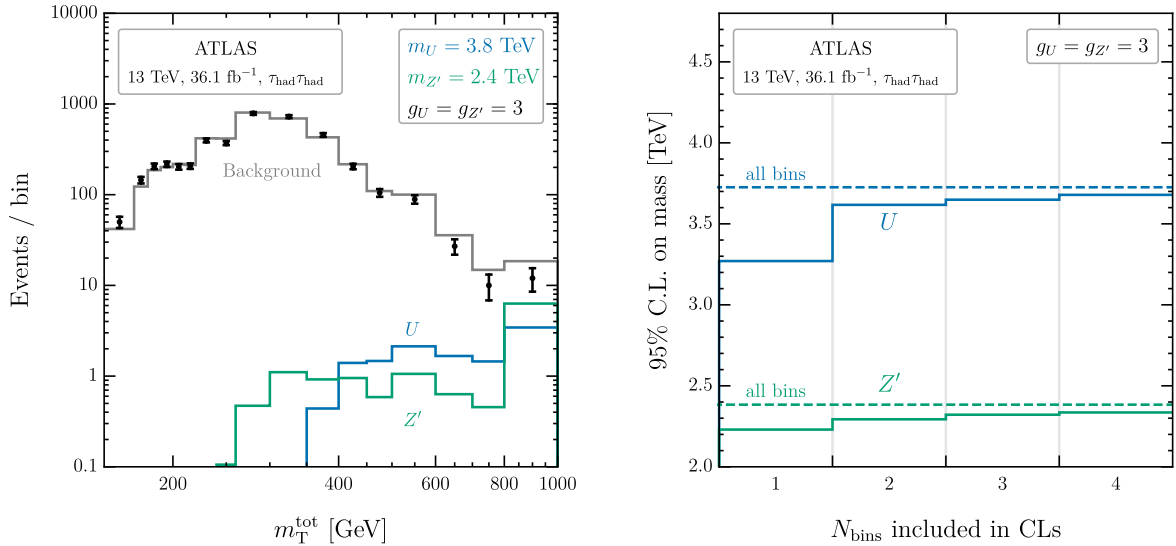


Figure 5: Left: Distributions in m_T^{tot} for the b -inclusive background and data from [43], a leptoquark (blue) and a Z' (green) with masses and couplings as shown. Right: The 95% C.L. on the mass of a leptoquark (blue) and a Z' (green) when only the highest N bins are included in the CLs, with couplings as shown. The dashed lines show the limit obtained when all bins are included.

Particle selection 1	No events with an electron ($p_T^e > 20$ GeV, $ \eta_e < 2.4$)
Particle selection 2	No events with a muon ($p_T^\mu > 20$ GeV, $ \eta_\mu < 2.5$)
$\tau_h p_T$	$p_T^{\tau_h} > 80$ GeV
Missing energy	$E_T^{\text{miss}} > 200$
p_T vs missing energy	$0.7 < p_T^{\tau_h} / E_T^{\text{miss}} < 1.3$
ϕ	$ \Delta\phi(p_T^{\tau_h}, p_T^{\text{miss}}) > 2.4$ rad

Table 4: Summary of the experimental cuts for the CMS $\tau_h \nu$ search [44].

tion of the τ final state is done with **Pythia 8.2** [60] using the CUETP8M1 set of tuned parameters. The detector response is simulated using **Delphes 3.4.1** [61]. The CMS Delphes card has been modified to satisfy the object reconstruction and identification requirements, in particular we include the τ -tagging efficiencies quoted in the experimental search [44].

After showering and detector simulation, we apply the selection cuts specified in table 4 using **MadAnalysis 5 v1.6.33** [62]. As a cross-check we have generated the SM Drell-Yan $pp \rightarrow \tau\nu$ background and compared our results to the one quoted by CMS. A good agreement is found between the two samples, within 20% of the quoted central values.

After passing through selection cuts, the resulting events are binned according to their total transverse mass,

$$m_T^{\text{tot}} \equiv \sqrt{2p_T^{\tau_h} p_T^{\text{miss}} [1 - \cos \Delta\phi(\vec{p}_T^{\tau_h}, \vec{p}_T^{\text{miss}})]}, \quad (15)$$

with $p_T^{\tau_h}$ and p_T^{miss} being, respectively, the transverse momenta of the visible decay products of the τ and the missing transverse momentum in the reconstructed event. We compare our binned events with the data and background estimates presented in fig. 3 (left) of [44]. For the statistical analysis we use the modified frequentist CL_s method [63] computed with the **ROOT** [64] package **Tlimit** [65].

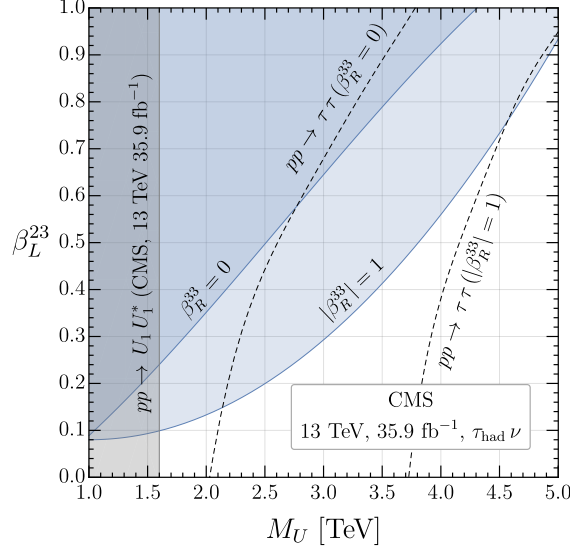


Figure 6: Exclusion limits from the $pp \rightarrow \tau\nu$ search in the (β_L^{23}, M_U) plane for different values of the coupling β_R^{33} . We fix $\beta_L^{33} = 1$, $g_U = 3$ and the leptoquark width to its natural value. The corresponding limits from $pp \rightarrow \tau\tau$ and pair-production, using the same parameter points, are overlaid.

In the determination of the limit, we include a systematic uncertainty of 20% in the NP signal to account for possible uncertainties related to the PDF, tau hadronization, detector simulation and unaccounted NLO corrections.

4.3.2 Limits on the U_1 leptoquark

For this search, we fix $\beta_L^{33} = 1$ and consider two different benchmarks for the right-handed coupling, $|\beta_R^{33}| = 0, 1$. In this case the relative sign between β_R^{33} and β_L^{33} is not observable in this channel. Since the leptoquark width plays a marginal role, we fix it to its natural value. We furthermore set $g_U = 3$.

We compute exclusion limits for the vector leptoquark in the (β_L^{23}, M_U) plane, see fig. 6. For comparison, we overlay the corresponding limits from $pp \rightarrow \tau\tau$ (see fig. 1 (right)) and pair-production limits. As can be seen, these limits give complementary information to those presented in section 4.2.2, offering more stringent limits only when the β_L^{23} coupling becomes large. Analogous limits for the case $\beta_R^{33} = 0$ have already been derived in the past literature [14]; we find good agreement between these limits and the ones quoted here. Interestingly, and as happens in the $pp \rightarrow \tau\tau$ search, the exclusion bounds get significantly affected by non-zero values of β_R^{33} . The different shapes in the exclusion bands can be understood from the fact that, for $|\beta_R^{33}| = 1$, the dominant partonic process is $bc \rightarrow \tau\nu$, whose cross section scales as $\sigma_{bc \rightarrow \tau\nu} \sim |\beta_L^{23}|^2/M_U^4$ in the EFT limit. On the contrary, for $\beta_R^{33} = 0$, the relative contribution from sc production, for which $\sigma_{sc \rightarrow \tau\nu} \sim (|\beta_L^{23}|/M_U)^4$, is important and even becomes dominant for medium-size values of β_L^{23} .

4.4 $pp \rightarrow \tau\mu$ search

The ATLAS collaboration has published a search for heavy particles decaying into different-flavour dilepton pairs using 36.1 fb^{-1} [45] of 13 TeV data. In this section we recast the ATLAS data and reinterpret the collider bounds in terms of the model in section 3 to set limits on β_{32}^L and ζ_ℓ^{23} , as a function of the leptoquark and Z' masses, respectively.

Particle selection	One single τ and μ , no electrons
p_T	$p_T^{\tau_h} > 65 \text{ GeV}, p_T^\mu > 65 \text{ GeV}$
η	$ \eta_{\tau_h} < 2.5$ excluding $1.37 < \eta_{\tau_h} < 1.52$; $ \eta_\mu < 2.4$
ϕ	$ \Delta\phi(\tau_h, \mu) > 2.7 \text{ rad}$
ΔR	$\Delta R(\tau_h, \mu) > 0.4$

Table 5: Summary of the experimental cuts for the ATLAS $\tau_h \mu$ search [45].

4.4.1 Search strategy

We use `Madgraph5_aMC@NLO v2.6.3.2` [58] with the `NNPDF23_lo_as_0119_qed` PDF set [59] to compute the NP contribution to the $pp \rightarrow \tau\mu$ process. The output is passed to `Pythia 8.2` [60] for tau hadronization and the detector effects are simulated with `Delphes 3.4.1` [61]. The ATLAS Delphes card has been adjusted to satisfy the object reconstruction and identification criteria in the search. In particular we have modified the muon efficiency and momentum resolution to match the *High- p_T* muon operating point, and adjusted the missing energy reconstruction to account for muon effects. We have further included the τ -tagging efficiencies quoted in the experimental search [45].

After showering and detector simulation, we apply the selection cuts specified in table 5 using `MadAnalysis 5 v1.6.33` [62]. The resulting events are binned according to their dilepton invariant mass. Following the approach described by ATLAS [45], the tau momentum is reconstructed from the magnitude of the missing energy and the momentum direction of the visible tau decay products. This approach relies on the fact that the momentum of the visible tau decay products and the neutrino momentum are nearly collinear.

In order to validate our procedure, we have simulated the Z' signal quoted in the experimental search [45], finding good agreement between our signal and the one by ATLAS.

We use the modified frequentist CL_s method [63] to obtain 95% CL limits. These limits are computed using the `ROOT` [64] package `Tlimit` [65]. In the determination of those limits, we include a systematic uncertainty of 20% for the NP signal to account for possible uncertainties related to the PDF, tau hadronization, detector simulation and unaccounted NLO corrections.

4.4.2 Limits on the U_1 leptoquark

Following a similar strategy as for the other channels, we fix $g_U = 3$ and $\beta_L^{33} = 1$, and take two benchmark values for the right-handed coupling $|\beta_R^{33}| = 0, 1$ (different sign choices for this parameter do not have an impact on the high- p_T signal). Varying the leptoquark width only yields a subleading effect so we keep it fixed to its natural value.

We decouple the Z' and compute the exclusion limits for the vector leptoquark mass as a function of β_L^{32} , see fig. 7 (left). As in previously analysed channels, the exclusion limits vary significantly for different values of β_R^{33} . We additionally overlay the corresponding exclusion limit obtained from the $pp \rightarrow \tau\tau$ search and searches for pair-production. The limits from $pp \rightarrow \tau\mu$ become stronger than those obtained from $pp \rightarrow \tau\tau$ only for large values of the β_L^{32} parameter, especially in the case when $|\beta_R^{33}| = 1$.

The limits presented here offer complementary constraints to the ones obtained from low-energy flavour observables. Interestingly, we find the current bounds from high- p_T data to be more constraining than those from its low energy counterpart, $\Upsilon \rightarrow \tau\mu$ (see e.g. [24]).⁶ Future improvements on this measurement can serve as a valuable probe of the leptoquark flavour structure.

⁶Current limits from loop-mediated transitions, such as $\tau \rightarrow \mu\gamma$, offer stronger bounds in certain UV completions [26]. However, these bounds are more sensitive to the details of the UV completion and are therefore less robust.

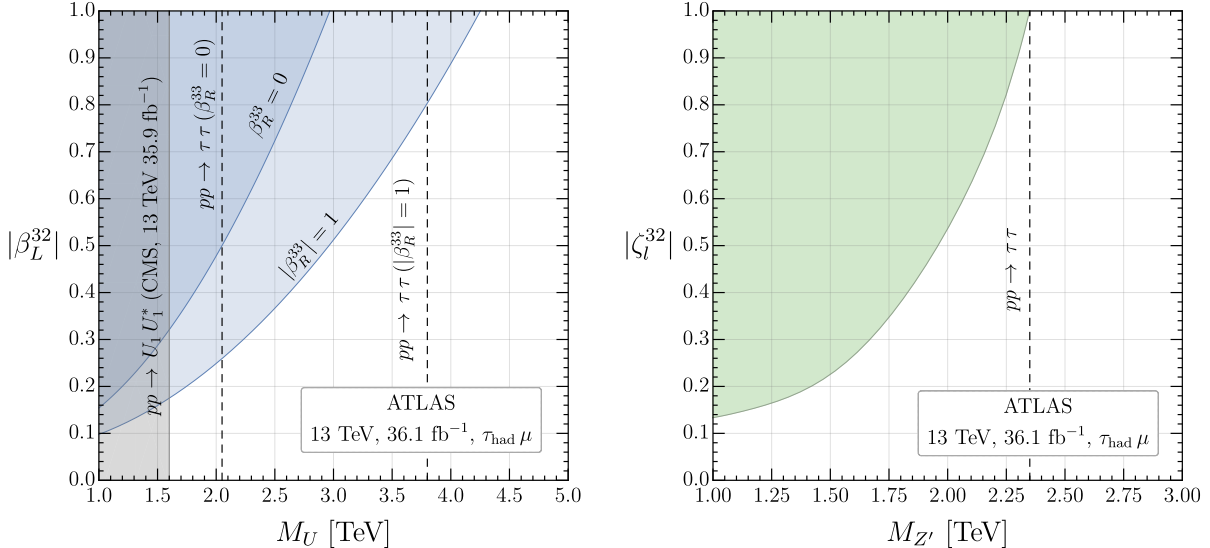


Figure 7: 95% CL exclusion limits from the $pp \rightarrow \tau\mu$ search. Left: U_1 limits in the (β_L^{32}, M_U) plane for different values of the coupling β_R^{33} . We fix $\beta_L^{33} = 1$, $g_U = 3$ and the leptoquark width to its natural value. Right: Z' limits in the $(\zeta_L^{32}, M_{Z'})$ plane, taking the natural width for the Z' and fixing $g_{Z'} = 3$. For comparison, the bounds from U_1 pair-production and from $pp \rightarrow \tau\tau$ are also shown.

4.4.3 Limits on the Z'

We finally comment on the limits on the Z' , decoupling the leptoquark. We fix $g_{Z'} = 3$, $\zeta_{q,u,d}^{33} = \zeta_{\ell,e}^{33} = 1$ and set the Z' width to its natural value. Limits on the Z' mass as a function of ζ_L^{32} are shown in fig. 7 (right). As in the leptoquark case, we overlay the corresponding limits on the Z' mass extracted from $pp \rightarrow \tau\tau$. As can be seen, these limits are always stronger than those from the present search, irrespective of the value of ζ_L^{32} .

4.5 $pp \rightarrow t\bar{t}$ search

We finally turn our attention to searches in the ditop final state, which is subject to NP effects from s channel colorons and Z' bosons. We focus our analysis on the coloron since the bounds from this channel on the Z' are weaker than the ones reported in section 4.2.3.

4.5.1 Search strategy

We perform a recast of the ATLAS study [46], using 36 fb^{-1} of collected data. Since the data was unfolded in this work, we can compute parton-level predictions and directly compare them to the unfolded distributions provided in the reference study.

We choose to derive the constraints from the normalised parton-level differential cross-sections as a function of the $t\bar{t}$ -invariant mass, shown in fig. 14(b) of [46]. Our signal predictions are derived by integrating the leading-order SM QCD partonic cross-sections $q\bar{q} \rightarrow t\bar{t}$ and $gg \rightarrow t\bar{t}$ and the NP contributions from coloron and Z' over the parton distribution functions, employing the `NNPDF30_nlo_as_0119` PDF set [59] and fixing the factorisation and renormalization scale to the center of the corresponding $t\bar{t}$ -invariant mass bin. We use the running strong coupling constant as provided by the PDF set. The only cut applied is on transverse momentum of either top quark: $p_T^t > 500$ GeV. Note that our reference study places the cuts as $p_T^{t,1} > 500$ GeV on the leading top, and $p_T^{t,2} > 350$ GeV on the subleading one. For a fully exclusive, partonic $t\bar{t}$ final state, $p_T^{t,1} = p_T^{t,2}$ and hence the second cut does

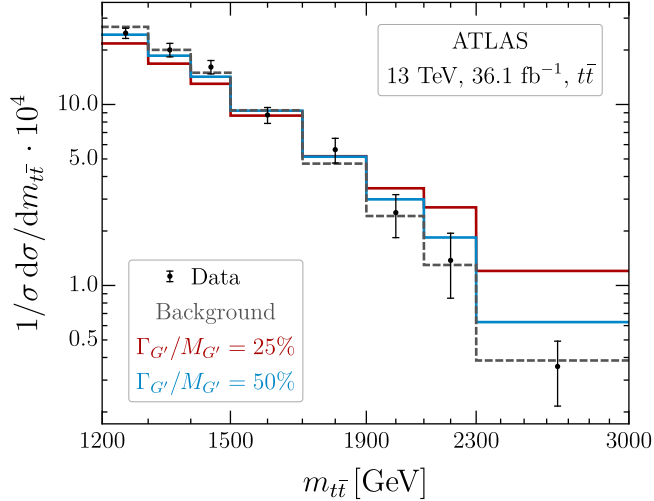


Figure 8: Illustration of the coloron signal in the ditop final state for $M_{G'} = 2.5$ TeV, $\kappa_q^{ll} = 0$, and two reference values for the width, compared to the data from [46].

not influence our calculation. However, the unfolded distributions are derived from data which employ this slightly milder cut, leading to slight deviations in bins of lower invariant mass. We therefore drop the bins $m_{t\bar{t}} < 1.2$ TeV and then find excellent agreement with the SM predictions presented in the ATLAS study. While the analysis also provides unfolded spectra differential in p_T and various other kinematic observables, we find the invariant mass spectrum to be the most constraining distribution. We therefore focus solely on the invariant mass spectrum and do not consider searches in the angular spectra.

4.5.2 Limits on the coloron

We are now ready to present the constraints on the various parameters related to the coloron. Throughout this section we set $\kappa_q^{33} = 1$ and $\kappa_q^{ll} = \kappa_u^{ll} = \kappa_d^{ll} = -(g_s/g_{G'})^2$, and we fix $g_{G'} = 3$, unless otherwise stated.

Before discussing each plot by itself, a few general comments are in order. Since the search is in a normalised spectrum, it is mostly sensitive to signals that create a shape sufficiently distinct to the background. A distinct shape in this case means a change in the spectrum that is unaffected by normalisation, meaning a peak or a change in the overall slope. Uniform shifts in the spectra (originating from resonances with both very high and very low masses, or large widths⁷) are washed out by the overall normalisation. As a result, the strongest bounds are obtained when the coloron can be produced nearly on-shell and the width is moderate. For example, in fig. 8 we show the signal of two parameter points with $\kappa_q^{ll} = 0$, $M_{G'} = 2.5$ TeV and different choices of the coloron width. We see that the narrower coloron results in a larger change in the slope.

In fig. 9, we show exclusion regions for the coloron with its natural width and with a width enhanced by a factor of two. In the left panel, the exclusion limits in the $(g_{G'}, M_{G'})$ plane are shown for the natural width and twice this value. An interesting feature of these exclusion regions is that the boundaries bend towards smaller masses for larger couplings. This can be understood by the fact that while the cross section grows with the coupling, so does the width. For the reasons discussed above, the search then loses sensitivity to the resulting signal.

In the right panel of fig. 9, exclusions are shown for varying values of the coupling to left-handed light quarks κ_q^{ll} , keeping the right-handed couplings $\kappa_{u,d}^{ll}$ fixed. With larger couplings to the light

⁷A very wide resonance also leads to a suppression in the overall signal cross-section, further decreasing the constraining power of the search.

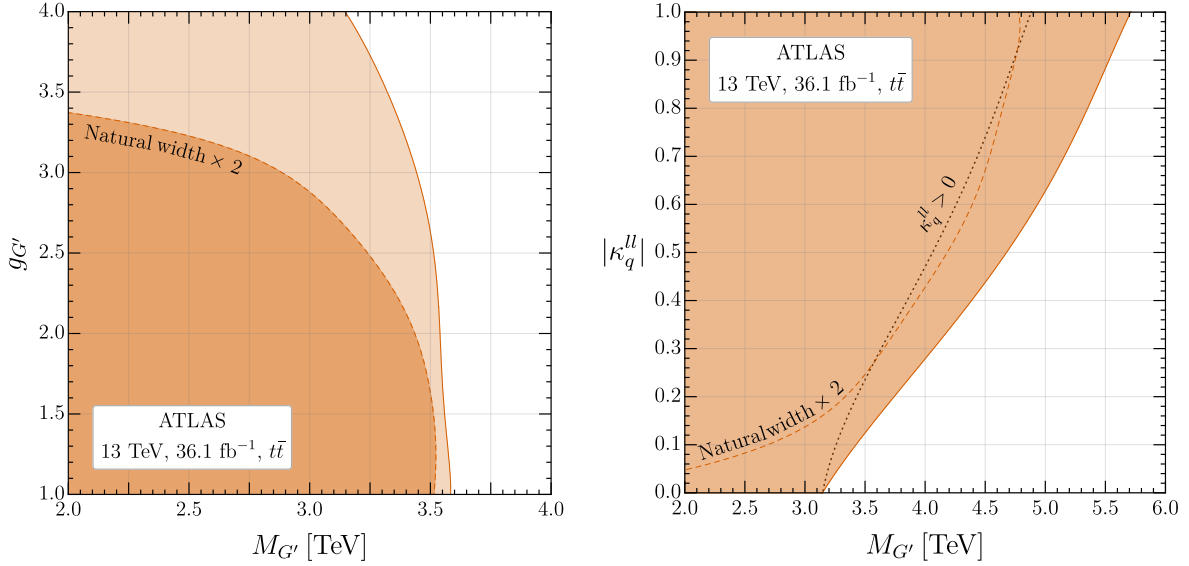


Figure 9: Left: Exclusion plot for the $pp \rightarrow t\bar{t}$ search in the $(g_{G'}, M_{G'})$ plane for the natural width (solid line) and twice the natural width (dashed line). Right: Exclusion limits on the coupling to light left-handed quarks κ_q^{ll} . The regions bounded by solid and dashed lines correspond to $\kappa_q^{ll} < 0$ with the natural width and twice the natural width, respectively. The dashed line denotes the exclusion region for $\kappa_q^{ll} > 0$.

quarks, the production of the coloron from valence quarks of the proton increases drastically. Since the valence quarks tend to carry more of the protons' momenta, they can produce the coloron closer to its mass shell, leading to a signal that the search can more easily discriminate from the background. If we were to set $\kappa_u^{ll} = \kappa_d^{ll} = \kappa_q^{ll} = 0$, we would find only very mild bounds, in which case the pair-production search discussed in section 4.1 outperforms this one. If κ_q^{ll} is chosen to be positive, the bounds tend to be weaker due to interference between the NP and the SM contributions.

Finally, fig. 10 shows exclusion limits with varying widths of the coloron. The different curves (solid, dashed, dotted) show various different choices of relations between the couplings to left- and right-handed light quarks. As expected, limits get weaker with increasing width of the resonance. When the sign of κ_q^{ll} is chosen to be opposite of $\kappa_{u,d}^{ll}$, the bounds also become weaker for the same reason as discussed above. The grey bands denote the regions in which the floating width parameter is below the partial width to quarks. Note that for $\kappa_{G'} \neq 0$ the coloron can decay to two gluons, in which case the actual width would become significantly larger than the partial width to quarks alone.⁸

5 Conclusions

The high- p_T phenomenology of models predicting a TeV-scale $SU(2)_L$ singlet vector leptoquark which is able to account for the hints of LFU violations observed in B -meson decays is quite rich. This is both because this exotic mediator can manifest itself in different final states accessible at the LHC, and also because this state cannot be the only TeV-scale exotic vector. As we have shown, the minimal consistent set of massive vectors comprising a U_1 also includes a coloron and a Z' . In this paper we

⁸In this case, the production cross section of the coloron would also be drastically increased, leading to much stronger bounds on its mass from this search.

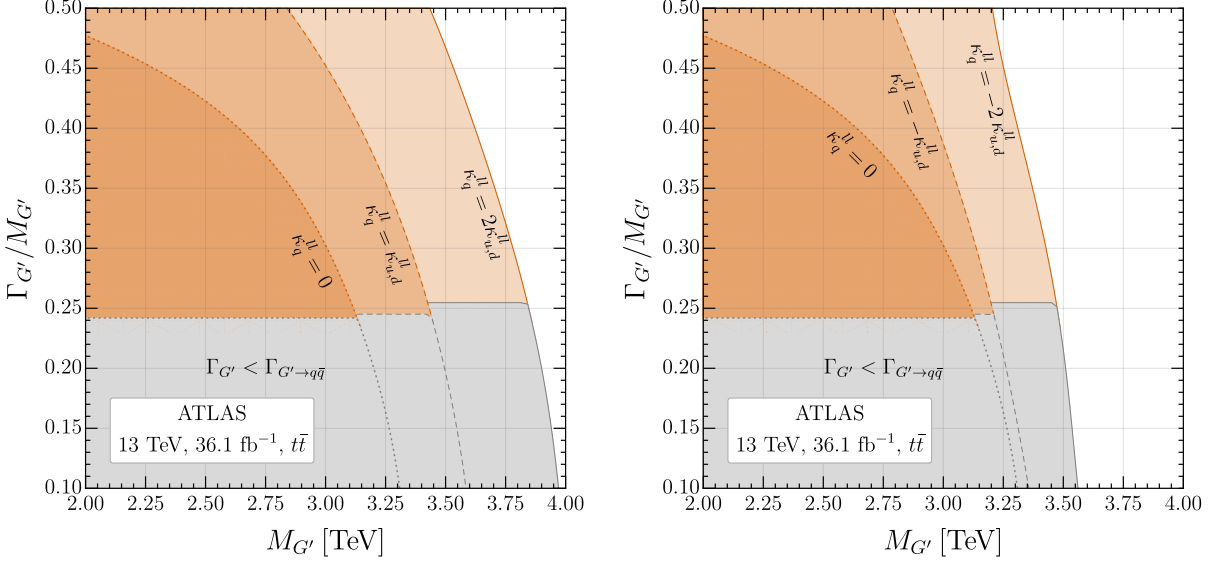


Figure 10: Exclusion limits on the coloron for the $pp \rightarrow t\bar{t}$ search in the $(\Gamma_{G'}/M_{G'}, M_{G'})$ plane for different choices of the couplings to light left-handed quarks.

have presented a comprehensive analysis of the high- p_T signatures of this set of exotic TeV states, deriving a series of bounds on their masses and couplings.

The results have been discussed in detail in the previous section and will not be repeated here. Here we limit ourself to summarise a few key messages, emphasising the novelties of our analysis compared to the results in the existing literature:

- In most of the relevant parameter space the most stringent bound on the leptoquark is obtained by the $pp \rightarrow \tau\tau$ process. In this channel a possible $O(1)$ right-handed coupling (β_R^{33}) has a very large impact, as shown in fig. 1.
- A non-vanishing off-diagonal coupling of the U_1 to quarks has a modest impact in $pp \rightarrow \tau\tau$, provided $|\beta_L^{23}| \lesssim 0.2$ (as expected from a natural flavour structure), but a significantly larger impact in $pp \rightarrow \tau\nu$. However, the latter search remains subleading compared to $pp \rightarrow \tau\tau$ up to $|\beta_L^{23}| \lesssim 0.8$ for $|\beta_R^{33}| = 1$ (or up to $|\beta_L^{23}| \lesssim 0.6$ for $|\beta_R^{33}| = 0$).
- For large non-vanishing off-diagonal coupling to leptons, a potentially interesting channel is $pp \rightarrow \tau\mu$. In the pure left-handed case, the bound from this channel is stronger than the one from $pp \rightarrow \tau\tau$ if $|\beta_L^{32}| \geq 0.5$ (see fig. 7).
- Taking $g_U = g_{Z'}$ and assuming dominant third-generation coupling to fermions and small couplings to the light families, the constraints on the Z' mass are significantly weaker than those on the U_1 (see fig. 4). The combination of U_1 and Z' signals in $pp \rightarrow \tau\tau$ leads to a modest increase on the corresponding bounds, confined to a relatively narrow region of the parameter space.
- The bound on the coloron from $pp \rightarrow t\bar{t}$ is quite sensitive to the width of this state, and to the possible coupling to light quarks. Due to the increase of the width, the bounds become weaker at large couplings (see fig. 10 (left)).

The bounds we have obtained are very general and can be applied to a large class of models. One of the advantages of having analysed the three states together is the possibility of performing a direct comparison of the bounds obtained from the different mediators (via different processes) on

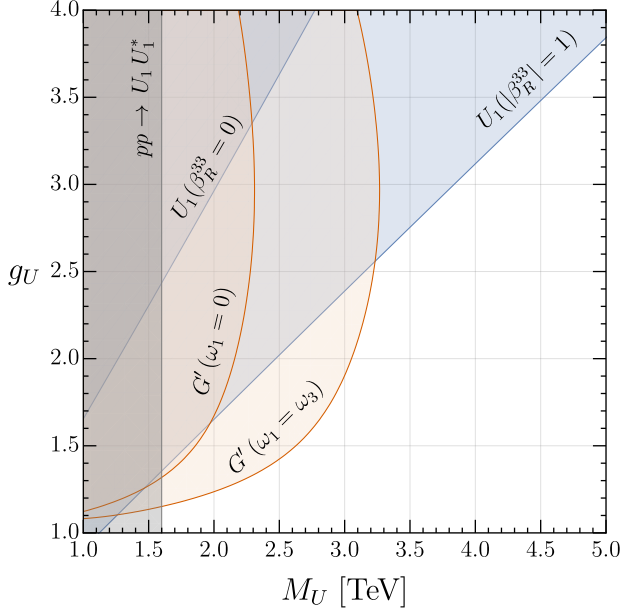


Figure 11: Leading 95% CL exclusion limits for the U_1 and the coloron, shown in the (g_U, M_U) plane assuming the relation between their masses and couplings following from the gauge symmetry in (6) and the breaking pattern assumed in [15, 18]. See text for more details.

the same model parameter space. As an illustration of this fact, in fig. 11 we show a comparison of U_1 and coloron bounds in the (g_U, M_U) plane, assuming the following relation between their masses and couplings

$$M_{G'} = M_U \frac{g_U}{\sqrt{g_U^2 - g_s^2}} \sqrt{\frac{2\omega_3^2}{\omega_1^2 + \omega_3^2}}, \quad g_{G'} = \sqrt{g_U^2 - g_s^2}. \quad (16)$$

This relation follows from the gauge symmetry in eq. (6) assuming two breaking terms transforming as $\omega_3 \sim (4, \bar{3})$ and $\omega_1 \sim (4, 1)$ under $SU(4) \times SU(3)'$ [15, 18]. As can be seen, there is an interesting interplay between the two types of bounds, which changes according to the (model-dependent) ratio ω_1/ω_3 . Once more, it is worth stressing the importance of the possible right-handed coupling of the U_1 (neglected in previous analyses): while the coloron sets the most stringent bounds on most of the parameter space for $\beta_{33}^R = 0$, this is no-longer true for $\beta_{33}^R = O(1)$. This implies a more direct connection between high- p_T physics and B -physics anomalies in models with a large right-handed coupling of the leptoquark.

Acknowledgements

We thank Claudia Cornellà and Admir Greljo for useful comments on the manuscript. JFM is grateful to the Mainz Institute for Theoretical Physics (MITP) for its hospitality and its partial support while this work was being finalised. We would like to thank Hubert Spiesberger for allowing us to use the THEP Cluster in Mainz for parts of this study. This research was supported in part by the Swiss National Science Foundation (SNF) under contract 200021-159720.

References

- [1] **BaBar** Collaboration, J. P. Lees et al., *Measurement of an Excess of $\bar{B} \rightarrow D^{(*)}\tau^-\bar{\nu}_\tau$ Decays and Implications for Charged Higgs Bosons*, *Phys. Rev.* **D88** (2013), no. 7 072012, [[arXiv:1303.0571](#)].
- [2] **LHCb** Collaboration, R. Aaij et al., *Measurement of the ratio of branching fractions $\mathcal{B}(\bar{B}^0 \rightarrow D^{*+}\tau^-\bar{\nu}_\tau)/\mathcal{B}(\bar{B}^0 \rightarrow D^{*+}\mu^-\bar{\nu}_\mu)$* , *Phys. Rev. Lett.* **115** (2015), no. 11 111803, [[arXiv:1506.08614](#)]. [Erratum: *Phys. Rev. Lett.* 115, no. 15, 159901 (2015)].
- [3] **Belle** Collaboration, S. Hirose et al., *Measurement of the τ lepton polarization and $R(D^*)$ in the decay $\bar{B} \rightarrow D^*\tau^-\bar{\nu}_\tau$* , *Phys. Rev. Lett.* **118** (2017), no. 21 211801, [[arXiv:1612.00529](#)].
- [4] **LHCb** Collaboration, R. Aaij et al., *Test of Lepton Flavor Universality by the measurement of the $B^0 \rightarrow D^{*-}\tau^+\nu_\tau$ branching fraction using three-prong τ decays*, *Phys. Rev. D97* (2018), no. 7 072013, [[arXiv:1711.02505](#)].
- [5] **LHCb** Collaboration, R. Aaij et al., *Test of lepton universality using $B^+ \rightarrow K^+\ell^+\ell^-$ decays*, *Phys. Rev. Lett.* **113** (2014) 151601, [[arXiv:1406.6482](#)].
- [6] **LHCb** Collaboration, R. Aaij et al., *Test of lepton universality with $B^0 \rightarrow K^{*0}\ell^+\ell^-$ decays*, *JHEP* **08** (2017) 055, [[arXiv:1705.05802](#)].
- [7] B. Bhattacharya, A. Datta, D. London, and S. Shivashankara, *Simultaneous Explanation of the R_K and $R(D^{(*)})$ Puzzles*, *Phys. Lett.* **B742** (2015) 370–374, [[arXiv:1412.7164](#)].
- [8] R. Alonso, B. Grinstein, and J. Martin Camalich, *Lepton universality violation and lepton flavor conservation in B -meson decays*, *JHEP* **10** (2015) 184, [[arXiv:1505.05164](#)].
- [9] A. Greljo, G. Isidori, and D. Marzocca, *On the breaking of Lepton Flavor Universality in B decays*, *JHEP* **07** (2015) 142, [[arXiv:1506.01705](#)].
- [10] L. Calibbi, A. Crivellin, and T. Ota, *Effective Field Theory Approach to $b \rightarrow s\ell(\ell')$, $B \rightarrow K(*)\nu\bar{\nu}$ and $B \rightarrow D(*)\tau\nu$ with Third Generation Couplings*, *Phys. Rev. Lett.* **115** (2015) 181801, [[arXiv:1506.02661](#)].
- [11] R. Barbieri, G. Isidori, A. Pattori, and F. Senia, *Anomalies in B -decays and $U(2)$ flavour symmetry*, *Eur. Phys. J.* **C76** (2016), no. 2 67, [[arXiv:1512.01560](#)].
- [12] D. A. Faroughy, A. Greljo, and J. F. Kamenik, *Confronting lepton flavor universality violation in B decays with high- p_T tau lepton searches at LHC*, *Phys. Lett.* **B764** (2017) 126–134, [[arXiv:1609.07138](#)].
- [13] A. Greljo and D. Marzocca, *High- p_T dilepton tails and flavor physics*, *Eur. Phys. J.* **C77** (2017), no. 8 548, [[arXiv:1704.09015](#)].
- [14] A. Greljo, J. Martin Camalich, and J. D. Ruiz-Alvarez, *The Mono-Tau Menace: From B Decays to High- p_T Tails*, [[arXiv:1811.07920](#)].
- [15] L. Di Luzio, A. Greljo, and M. Nardecchia, *Gauge leptoquark as the origin of B -physics anomalies*, *Phys. Rev.* **D96** (2017), no. 11 115011, [[arXiv:1708.08450](#)].
- [16] N. Assad, B. Fornal, and B. Grinstein, *Baryon Number and Lepton Universality Violation in Leptoquark and Diquark Models*, *Phys. Lett.* **B777** (2018) 324–331, [[arXiv:1708.06350](#)].
- [17] L. Calibbi, A. Crivellin, and T. Li, *Model of vector leptoquarks in view of the B -physics anomalies*, *Phys. Rev.* **D98** (2018), no. 11 115002, [[arXiv:1709.00692](#)].
- [18] M. Bordone, C. Cornella, J. Fuentes-Martin, and G. Isidori, *A three-site gauge model for flavor hierarchies and flavor anomalies*, *Phys. Lett.* **B779** (2018) 317–323, [[arXiv:1712.01368](#)].
- [19] R. Barbieri and A. Tesi, *B -decay anomalies in Pati-Salam $SU(4)$* , *Eur. Phys. J.* **C78** (2018), no. 3 193, [[arXiv:1712.06844](#)].
- [20] A. Greljo and B. A. Stefanek, *Third family quark-lepton unification at the TeV scale*, *Phys. Lett.* **B782** (2018) 131–138, [[arXiv:1802.04274](#)].
- [21] M. Blanke and A. Crivellin, *B Meson Anomalies in a Pati-Salam Model within the Randall-Sundrum Background*, *Phys. Rev. Lett.* **121** (2018), no. 1 011801, [[arXiv:1801.07256](#)].
- [22] L. Di Luzio, J. Fuentes-Martin, A. Greljo, M. Nardecchia, and S. Renner, *Maximal Flavour Violation: a Cabibbo mechanism for leptoquarks*, *JHEP* **11** (2018) 081, [[arXiv:1808.00942](#)].
- [23] D. Marzocca, *Addressing the B -physics anomalies in a fundamental Composite Higgs Model*, *JHEP* **07** (2018) 121, [[arXiv:1803.10972](#)].
- [24] J. Kumar, D. London, and R. Watanabe, *Combined Explanations of the $b \rightarrow s\mu^+\mu^-$ and $b \rightarrow c\tau^-\bar{\nu}$ Anomalies: a General Model Analysis*, *Phys. Rev.* **D99** (2019), no. 1 015007, [[arXiv:1806.07403](#)].
- [25] D. Becirevic, I. Dorsner, S. Fajfer, N. Kosnik, D. A. Faroughy, and O. Sumensari, *Scalar leptoquarks from grand unified theories to accommodate the B -physics anomalies*, *Phys. Rev.* **D98** (2018), no. 5 055003, [[arXiv:1806.05689](#)].
- [26] M. Bordone, C. Cornella, J. Fuentes-Martin, and G. Isidori, *Low-energy signatures of the PS^3 model: from B -physics anomalies to LFV*, *JHEP* **10** (2018) 148, [[arXiv:1805.09328](#)].
- [27] B. Fornal, S. A. Gadom, and B. Grinstein, *Left-Right $SU(4)$ Vector Leptoquark Model for Flavor Anomalies*, [[arXiv:1812.01603](#)].
- [28] D. Buttazzo, A. Greljo, G. Isidori, and D. Marzocca, *B -physics anomalies: a guide to combined explanations*, *JHEP* **11** (2017) 044, [[arXiv:1706.07808](#)].

[29] J. C. Pati and A. Salam, *Lepton Number as the Fourth Color*, *Phys. Rev.* **D10** (1974) 275–289. [Erratum: *Phys. Rev.* D11, 703 (1975)].

[30] **CMS** Collaboration, A. M. Sirunyan et al., *Search for high-mass resonances in dilepton final states in proton-proton collisions at $\sqrt{s} = 13$ TeV*, *JHEP* **06** (2018) 120, [[arXiv:1803.06292](#)].

[31] **ATLAS** Collaboration, M. Aaboud et al., *Search for new high-mass phenomena in the dilepton final state using 36 fb^{-1} of proton-proton collision data at $\sqrt{s} = 13$ TeV with the ATLAS detector*, *JHEP* **10** (2017) 182, [[arXiv:1707.02424](#)].

[32] H. Georgi and Y. Nakai, *Diphoton resonance from a new strong force*, *Phys. Rev.* **D94** (2016), no. 7 075005, [[arXiv:1606.05865](#)].

[33] B. Diaz, M. Schmaltz, and Y.-M. Zhong, *The leptoquark Hunter's guide: Pair production*, *JHEP* **10** (2017) 097, [[arXiv:1706.05033](#)].

[34] S. Iguro and Y. Omura, *Status of the semileptonic B decays and muon g-2 in general 2HDMs with right-handed neutrinos*, *JHEP* **05** (2018) 173, [[arXiv:1802.01732](#)].

[35] P. Asadi, M. R. Buckley, and D. Shih, *It's all right-handed neutrinos): a new W' model for the $R_{D^{(*)}}$ anomaly*, *JHEP* **09** (2018) 010, [[arXiv:1804.04135](#)].

[36] A. Greljo, D. J. Robinson, B. Shakya, and J. Zupan, *$R(D^{(*)})$ from W' and right-handed neutrinos*, *JHEP* **09** (2018) 169, [[arXiv:1804.04642](#)].

[37] D. J. Robinson, B. Shakya, and J. Zupan, *Right-handed Neutrinos and $R(D^{(*)})$* , [[arXiv:1807.04753](#)].

[38] A. Azatov, D. Barducci, D. Ghosh, D. Marzocca, and L. Ubaldi, *Combined explanations of B-physics anomalies: the sterile neutrino solution*, *JHEP* **10** (2018) 092, [[arXiv:1807.10745](#)].

[39] R. Barbieri, G. Isidori, J. Jones-Perez, P. Lodone, and D. M. Straub, *$U(2)$ and Minimal Flavour Violation in Supersymmetry*, *Eur. Phys. J.* **C71** (2011) 1725, [[arXiv:1105.2296](#)].

[40] **CMS** Collaboration, A. M. Sirunyan et al., *Search for heavy neutrinos and third-generation leptoquarks in hadronic states of two τ leptons and two jets in proton-proton collisions at $\sqrt{s} = 13$ TeV*, Submitted to: *JHEP* (2018) [[arXiv:1811.00806](#)].

[41] **CMS** Collaboration, C. Collaboration, *Constraints on models of scalar and vector leptoquarks decaying to a quark and a neutrino at $\sqrt{s} = 13$ TeV*, .

[42] **CMS** Collaboration, A. M. Sirunyan et al., *Search for pair-produced resonances decaying to quark pairs in proton-proton collisions at $\sqrt{s} = 13$ TeV*, *Phys. Rev.* **D98** (2018), no. 11 112014, [[arXiv:1808.03124](#)].

[43] **ATLAS** Collaboration, M. Aaboud et al., *Search for additional heavy neutral Higgs and gauge bosons in the ditau final state produced in 36 fb^{-1} of pp collisions at $\sqrt{s} = 13$ TeV with the ATLAS detector*, *JHEP* **01** (2018) 055, [[arXiv:1709.07242](#)].

[44] **CMS** Collaboration, A. M. Sirunyan et al., *Search for a W' boson decaying to a τ lepton and a neutrino in proton-proton collisions at $\sqrt{s} = 13$ TeV*, Submitted to: *Phys. Lett.* (2018) [[arXiv:1807.11421](#)].

[45] **ATLAS** Collaboration, M. Aaboud et al., *Search for lepton-flavor violation in different-flavor, high-mass final states in pp collisions at $\sqrt{s} = 13$ TeV with the ATLAS detector*, Submitted to: *Phys. Rev.* (2018) [[arXiv:1807.06573](#)].

[46] **ATLAS** Collaboration, M. Aaboud et al., *Measurements of $t\bar{t}$ differential cross-sections of highly boosted top quarks decaying to all-hadronic final states in pp collisions at $\sqrt{s} = 13$ TeV using the ATLAS detector*, *Phys. Rev.* **D98** (2018), no. 1 012003, [[arXiv:1801.02052](#)].

[47] J. Blumlein, E. Boos, and A. Kryukov, *Leptoquark pair production in hadronic interactions*, *Z. Phys.* **C76** (1997) 137–153, [[hep-ph/9610408](#)].

[48] **CMS** Collaboration, A. M. Sirunyan et al., *Search for additional neutral MSSM Higgs bosons in the $\tau\tau$ final state in proton-proton collisions at $\sqrt{s} = 13$ TeV*, *JHEP* **09** (2018) 007, [[arXiv:1803.06553](#)].

[49] **CMS** Collaboration, A. M. Sirunyan et al., *Search for narrow and broad dijet resonances in proton-proton collisions at $\sqrt{s} = 13$ TeV and constraints on dark matter mediators and other new particles*, *JHEP* **08** (2018) 130, [[arXiv:1806.00843](#)].

[50] **CMS** Collaboration, C. Collaboration, *Searches for dijet resonances in pp collisions at $\sqrt{s} = 13$ TeV using the 2016 and 2017 datasets*, .

[51] **ATLAS** Collaboration, M. Aaboud et al., *Search for low-mass dijet resonances using trigger-level jets with the ATLAS detector in pp collisions at $\sqrt{s} = 13$ TeV*, *Phys. Rev. Lett.* **121** (2018), no. 8 081801, [[arXiv:1804.03496](#)].

[52] **CMS** Collaboration, A. M. Sirunyan et al., *Search for narrow resonances in the b-tagged dijet mass spectrum in proton-proton collisions at $\sqrt{s} = 8$ TeV*, *Phys. Rev. Lett.* **120** (2018), no. 20 201801, [[arXiv:1802.06149](#)].

[53] **ATLAS** Collaboration, M. Aaboud et al., *Search for resonances in the mass distribution of jet pairs with one or two jets identified as b-jets in proton-proton collisions at $\sqrt{s} = 13$ TeV with the ATLAS detector*, *Phys. Rev.* **D98** (2018) 032016, [[arXiv:1805.09299](#)].

[54] A. Alloul, N. D. Christensen, C. Degrande, C. Duhr, and B. Fuks, *FeynRules 2.0 - A complete toolbox for tree-level phenomenology*, *Comput. Phys. Commun.* **185** (2014) 2250–2300, [[arXiv:1310.1921](#)].

[55] J. Aebischer, A. Crivellin, and C. Greub, *QCD Improved Matching for Semi-Leptonic B Decays with Leptoquarks*, [[arXiv:1811.08907](#)].

[56] I. Doršner and A. Greljo, *Leptoquark toolbox for precision collider studies*, *JHEP* **05** (2018) 126, [[arXiv:1801.07641](#)].

[57] A. Angelescu, D. Bećirević, D. A. Faroughy, and O. Sumensari, *Closing the window on single leptoquark solutions to the B-physics anomalies*, *JHEP* **10** (2018) 183, [[arXiv:1808.08179](https://arxiv.org/abs/1808.08179)].

[58] J. Alwall, R. Frederix, S. Frixione, V. Hirschi, F. Maltoni, O. Mattelaer, H. S. Shao, T. Stelzer, P. Torrielli, and M. Zaro, *The automated computation of tree-level and next-to-leading order differential cross sections, and their matching to parton shower simulations*, *JHEP* **07** (2014) 079, [[arXiv:1405.0301](https://arxiv.org/abs/1405.0301)].

[59] R. D. Ball et al., *Parton distributions with LHC data*, *Nucl. Phys.* **B867** (2013) 244–289, [[arXiv:1207.1303](https://arxiv.org/abs/1207.1303)].

[60] T. Sjöstrand, S. Ask, J. R. Christiansen, R. Corke, N. Desai, P. Ilten, S. Mrenna, S. Prestel, C. O. Rasmussen, and P. Z. Skands, *An Introduction to PYTHIA 8.2*, *Comput. Phys. Commun.* **191** (2015) 159–177, [[arXiv:1410.3012](https://arxiv.org/abs/1410.3012)].

[61] **DELPHES 3** Collaboration, J. de Favereau, C. Delaere, P. Demin, A. Giannanco, V. Lemaître, A. Mertens, and M. Selvaggi, *DELPHES 3, A modular framework for fast simulation of a generic collider experiment*, *JHEP* **02** (2014) 057, [[arXiv:1307.6346](https://arxiv.org/abs/1307.6346)].

[62] B. Dumont, B. Fuks, S. Kraml, S. Bein, G. Chalons, E. Conte, S. Kulkarni, D. Sengupta, and C. Wyman, *Toward a public analysis database for LHC new physics searches using MADANALYSIS 5*, *Eur. Phys. J.* **C75** (2015), no. 2 56, [[arXiv:1407.3278](https://arxiv.org/abs/1407.3278)].

[63] A. L. Read, *Presentation of search results: The $CL(s)$ technique*, *J. Phys.* **G28** (2002) 2693–2704. [,11(2002)].

[64] R. Brun and F. Rademakers, *ROOT: An object oriented data analysis framework*, *Nucl. Instrum. Meth.* **A389** (1997) 81–86.

[65] T. Junk, *Confidence level computation for combining searches with small statistics*, *Nucl. Instrum. Meth.* **A434** (1999) 435–443, [[hep-ex/9902006](https://arxiv.org/abs/hep-ex/9902006)].

[66] M. Schmaltz and Y.-M. Zhong, *The Leptoquark Hunter’s Guide: Large Coupling*, [arXiv:1810.10017](https://arxiv.org/abs/1810.10017).

[67] **ATLAS** Collaboration, M. Aaboud et al., *Search for High-Mass Resonances Decaying to $\tau\nu$ in pp Collisions at $\sqrt{s}=13$ TeV with the ATLAS Detector*, *Phys. Rev. Lett.* **120** (2018), no. 16 161802, [[arXiv:1801.06992](https://arxiv.org/abs/1801.06992)].